Sensors and Materials, Vol. 35, No. 8 (2023) 2705–2727
MYU Tokyo

S & M 3349

A Novel Design Optimization Methodology for Machine Tools Based on Computer-assisted Engineering and Sensor-based Measurement Techniques

Hao Ma, Kun-Chieh Wang,* and Chi-Hsin Yang

School of Mechanical and Electric Engineering, Sanming University, Sanming, Fujian Province 365004, China

(Received April 7, 2023; accepted July 31, 2023)

Keywords: machine tools, static stiffness, dynamic stiffness, mode shape, sensor technology

Structural rigidity is a crucial factor that determines machining accuracy for computer-numerical-controlled (CNC) machines. Therefore, how to design a highly rigid CNC machine tool has been the focus of attention. In response to the rapid changes in various machine tools attributable to market needs, it is necessary to find an efficient way to examine and optimally design their structures. In this study, we propose an optimization methodology based on the finite element method (FEM) and sensor-based measurement to efficiently investigate and obtain an optimal structure with high rigidity of the selected target CNC movable-cross-beam double-column machining center (MDMC). The proposed methodology is mainly composed of the prototype design of a target machine, theoretical investigations via FEM, static as well as dynamic stiffness analysis, experimental measurements based on sensors, investigations on crucial parameters that mostly affect the whole structural strength, and the design of an optimum structure via synthesis and comparison. We found that a reduction as large as 1000 mm in the Z travel of a spindle head causes decreases as large as 69.37% in minimum static stiffness and 37.93% in minimum dynamic stiffness. It is suggested that, for optimally designing our target MDMC, the Z-travel length of the spindle head should be reduced to half the original size. This proposed methodology is a rapid, effective, and economical way to optimally design or modify the structure of a MDMC. It can also be used as an optimization guide of the structural design for other types of CNC machine tool.

1. Introduction

To properly design a high-precision computer-numerical-controlled (CNC) machine tool, it is vital that structural rigidity plays the most important role. However, the structures of CNC machine tools are becoming increasingly asymmetric and far more complicated than ever owing to changes in market needs. Among various CNC cutting machines, the column-type machining center is very popular because of its capability in stably cutting large and heavy machine parts. However, there are still some disadvantages in the structures of these types of machine, which

*Corresponding author: e-mail: m18316252102@126.com
https://doi.org/10.18494/SAM4442

ISSN 0914-4935
https://myukk.org/

remain unsolved, such as failures caused by resonance or large deformations due to the large extension length of structural components. On the other hand, to quickly respond to market changes in CNC machine tool trading, we need an efficient, rapid, and economical design methodology to optimally design a new or redesign an old CNC machine tool. Generally, there are two types of cutting force in the machining process, static and dynamic. The static force affects the geometric accuracy of work pieces, whereas the dynamic force affects the surface roughness of work pieces. Deformations occur when the machine structure is subject to these cutting forces. For a machine, static (dynamic) rigidity is defined as the applied static (dynamic) force divided by its resultant deformation. Traditionally, only the static rigidity is taken into consideration in designing a CNC machine. However, with the increasing demand for machining accuracy, the deformation induced by dynamic vibrations or resonances should no longer be ignored since they usually cause an inaccuracy of work piece dimension or, even worse, damage to the machine structure. Therefore, the goal of designing a strong CNC machine tool should be focused on how to obtain an optimal structure that exhibits high static as well as dynamic rigidity.

Many methodologies for optimizing the components of a CNC machine tool have been proposed, such as moving modules, the spindle, the machine bed, or vertical columns.[1–5] Conventionally, scholars used the static analysis method to investigate the optimization problems for the whole machine structure. Chen *et al*.[6] analyzed the design optimization problem for the machine structure with granite material. Wang *et al*.[7] performed a static analysis that explores the effect of static stiffness for an individual component on the whole static stiffness of a CNC vertical lathe with a steel-polymer concrete structure. Wang *et al*.[8] used static mechanics to design and develop a five-axis machine tool. Their studies focused on the method of how to design a machine with high static stiffness. Wu *et al*.[9] proposed a robust design optimization method for enhancing the static accuracy of a CNC vertical machining center. Petrea and Stan[10] adopted a static analysis based on the topological optimization method to investigate the structure of a Gantry-type CNC machine using the finite element analysis (FEA). Their results showed that the proposed optimization method may reduce the structural inertial forces by up to 30% while keeping the static rigidity unchanged. Thus far, the known popular optimization methods for designing CNC machine tools included the multiple-attribute decision-making method,[11] computer-assisted engineering (CAE) simulations,[12] the multidisciplinary approach,[13] and the tolerance modeling method,[14] which all considered the static rigidity as the target parameter.

With the increasing requirement on the machining accuracy up to the nanometer level for CNC machine tools, scholars have spent more energy than ever on investigating the issue of how to increase the dynamic stiffness of CNC machine tools. Liusheng *et al*.[15] investigated the optimization problem of a CNC lathe using dynamic characteristic analysis. Guo *et al*.[16] put forward a dynamic response approach to investigate the design optimization problem of the spindle of a CNC grinding machine. Son *et al*.[17] made a dynamic analysis of the optimal design for an arch-type desktop reconfigurable machine. Shi *et al*.[18] proposed a novel top-down design methodology for the rigidity of CNC machine tools. Das *et al*.[19] developed a new method to investigate the vibration-free machine structure for a machining center. Jie[20] proposed a

surface-response method to obtain an optimal structure of a CNC vertical machine tool. From the above survey results, we concluded that a synchronous consideration of both the static stiffness and dynamic stiffness of the whole machine structure is a prerequisite for designing an optimal CNC machine tool with high rigidity.

For a machine structure, the static stiffness is its deformation resistance when subjected to a static force. The modal shape is defined as the resultant deformation occurring at different natural frequencies. The dynamic stiffness is its deformation resistance when subjected to the external periodic stimuli of dynamic forces. The above three parameters significantly affect the rigidity of the whole machine. A synchronous examination of their effects on the machine structure is of marked importance to optimally design a CNC machine tool.

In this study, we intend to propose a novel optimization methodology based on the finite element method (FEM) and the sensor-based measurement to efficiently investigate, identify, and obtain an optimal structure of the target CNC movable-cross-beam double-column machining center (MDMC). The proposed methodology is a top-down sequential optimization design concept that mainly includes the initial prototype design, a synchronous consideration of the effects from three aforementioned crucial parameters, experimental verifications, and structural optimization. The reason for choosing this type of CNC machine tool is that its cross beam as well as vertical columns have crucial effects on the static as well as dynamic features of the machine.

2. Methodology

Our proposed optimization methodology consists of the following seven steps, as demonstrated in Fig. 1.

Step 1: Target selection. We choose a specific type of CNC machine tool as the target in which it has a movable cross beam, two vertical columns, and an extended spindle ram machine. This type of machine usually has the defects of large vibrations as well as deformations during machining.

Step 2: Initial design. We initially choose the designed CNC MDMC, No. SCR-5229 HLA, produced by SIGMA Co., Ltd., as the target machine, which is very popular in the market around the world, as shown in Fig. 2.

Step 3: Theoretical investigation. The related solid mechanics theories are introduced as the theoretical foundation for calculations of the static stiffness, mode shape, and dynamic stiffness. Note that we take into consideration the spindle-module position as the independent parameter in stiffness calculations.

Step 4: Static response analysis. After setting the applying force, the parameters of structural deformation, strain, and stress are calculated. The static stiffness of the whole machine is then obtained accordingly.

Step 5: Dynamic response analysis. After setting the applying periodic stimuli, the parameters of structural deformation, strain, and stress are calculated. The dynamic stiffness of the whole machine is obtained accordingly. Moreover, the modal shapes of free oscillations are calculated.

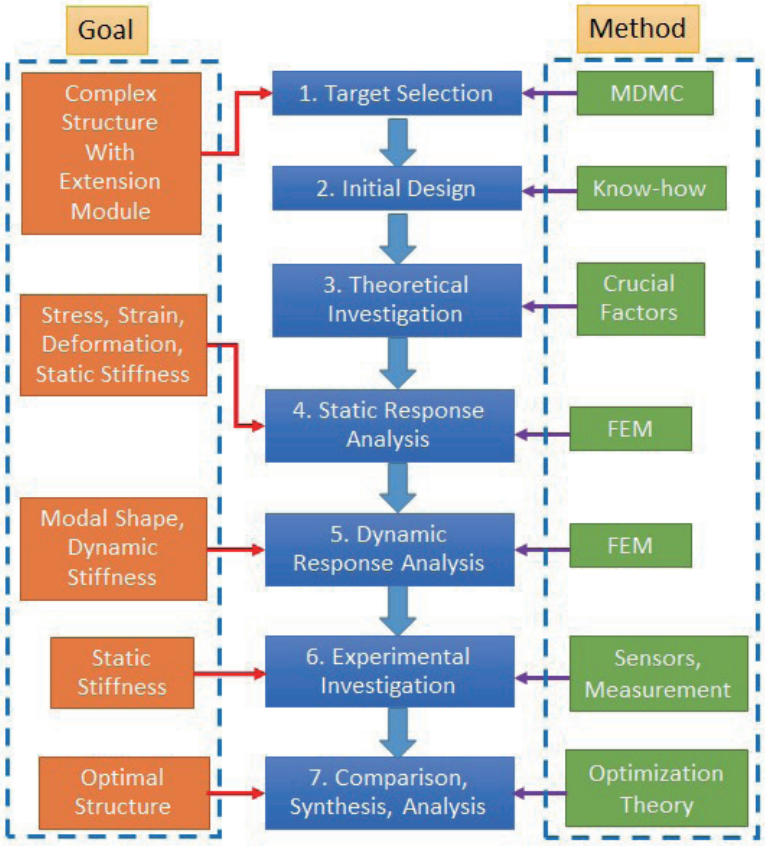

Fig. 1. (Color online) Flow chart of proposed optimization methodology.

Fig. 2. (Color online) Target CNC MDMC in market (produced by SIGMA Co., Ltd.).

Step 6: Experimental investigation. The experimental apparatus is set up and strain gauge sensors are mounted on the CNC MDMC. Some deformation measurements and investigations are performed.

Step 7: Synthesis, comparison, and analysis. By analyzing the obtained theoretical and experimental data, we propose an optimal design guide of the target CNC MDMC.

3. Foundation of Theory

The principles of solid mechanics used in this study consist of three aspects: statics, vibration theory, and kinematics. The detailed descriptions are as follows.

3.1 Principle of statics

When an object is subject to a load, the equation of force balance can be expressed in matrix form as

$$[S]\{D\} = \{P\}, \tag{1}$$

or

$$[S]\{D\} = \{P_e\} + \{P_r\}, \tag{2}$$

where $[S]$ is the static stiffness matrix of the system, $[S] = \sum_{i=1}^{m} [S_i]$; $\{D\}$ is the displacement vector; m is the element number; $[P_r]$ and $[P_e]$ are the reaction load and external force vectors, respectively. From this time on, the stress can be determined using the formula $\sigma = P/A$ and the strain $\varepsilon = D/l$, where A and l are respectively the characteristic area and length, with a relation of $\sigma = E\varepsilon$, where E is the elasticity modulus.

3.2 Vibration theory - modal analysis

The natural frequency and associated modal shape of a system can be obtained via modal analysis. The modal analysis gives engineers an idea of how the design will respond to different types of dynamic load. For the modal analysis without damping in this study, it is assumed that the structural material has constant physical properties and is linear in elasticity and free from loads. Since there is no force applied to the structure, the machine can be viewed as under free oscillation. The governing equation of the free oscillation for a linear structure without damping is

$$[M]\{\ddot{D}\} + [S]\{D\} = \{0\}. \tag{3}$$

Assuming that the structure is in harmonic motion, the displacement has the form

$$\{D\} = \{\phi\}_i \sin(\omega_i t + \theta_i), \tag{4}$$

where $\{\phi\}_i$ is the amplitude for the ith frequency ω_i. Substituting Eq. (4) into Eq. (3), we obtain

$$\left[\left[S\right]-\omega_i^2\left[M\right]\right]\{\phi\}_i=\{0\}\,. \tag{5}$$

To obtain a nontrivial solution, the following condition must be satisfied:

$$\det\left(\ \left[\left[S\right]-\omega_i^2\left[M\right]\right]\ \right)=0\,. \tag{6}$$

On the basis of Eq. (6), we obtain the natural frequencies $\{\omega_i\}$ or $\{f_i\}$, where $f_i = \omega_i/2\pi$ (unit: Hz), and their corresponding modal shapes $\{\phi\}$.

3.3 Principle of kinematics

From Newton's second law, when a machine structure is subject to a time-variant force $\{P(t)\}$, the governing equation of the force balance can be written as

$$\left[M\right]\{\ddot{D}\}+\left[C\right]\{\dot{D}\}+\left[S\right]\{D\}=\{P(t)\}\,, \tag{7}$$

where $[C]$ is the damping matrix. We assume that

$$\{P(t)\}=\{P_{\max}e^{i\psi}\}e^{i\omega t}\,, \tag{8}$$

and

$$\{D(t)\}=\{D_{\max}e^{i\theta}e^{i\omega t}\}\,, \tag{9}$$

where $P_{\max}$ is the maximum applied external force, ψ is the phase angle of the applied force, $D_{\max}$ is the maximum resultant displacement, and θ is the phase angle of the resultant displacement. Substituting Eqs. (8) and (9) into Eq. (7), we obtain the following equation:

$$(-\omega^2\left[M\right]+i\omega\left[C\right]+\left[S\right])\left\{D_{\max}e^{i\theta}\right\}=\left\{P_{\max}e^{i\psi}\right\}\,. \tag{10}$$

The final resultant displacement vector $\{D_{\max}e^{i\theta}\}$ is obtained by solving Eq. (10).

4. Results and Discussion

First, we carry out theoretical investigations on the selected target of a CNC MDMC through FEM calculations based on Eqs. (1) to (10). The content of investigations consists of the static stiffness, modal shapes, and dynamic stiffness of this machine structure. The position of the

center of gravity significantly affects the stability of a machine as well as its machining precision. Moreover, the spindle position in the ram plays a decisive role in determining the instantaneous location of the center of gravity for the whole machine. Therefore, here, we specifically study the effect of the spindle position in the ram on the machine's stiffness. Immediately after, we perform experimental studies by measuring deformations with force and displacement sensors and compare them with the results obtained by FEM. Some important findings and comments for designing an optimal structure of the target MDMC are drawn from the comparison results.

4.1 Theoretical study

The target machine's structure primarily contains a spindle ram, a cross beam, and two vertical columns, as shown in Fig. 3(a). Three representative spindle head locations, where the downward direction is positive, which consist of $Z = 0$ mm (top, Case A), $Z = 550$ mm (middle, Case B), and $Z = 1100$ mm (bottom, Case C), are taken into consideration. The bed structure of the target machine is not shown here since it has almost no deformation when the machine withstands external forces. Then, we conduct a grid-independent test, and the proper meshing result of a total of 421507 node numbers and 225137 elements is obtained [shown in Fig. 3(b)]. The boundary conditions for all cases are set such that the machine bed under both vertical columns has no deformation and all external forces are applied to the tip of the spindle nose. Cast iron is chosen as the structural material. Calculations via FEM are then performed to obtain the stiffness as well as the modal shape for the whole machine.

4.1.1 Static stress, strain, and deformation distributions (Case A)

We now examine Case A in which the spindle module just locates at the top position in the ram ($Z = 0$ mm). In this posture, an external force of $P_x = 100$ kg_f is applied to the spindle nose in the X direction. Through FEM calculations, the obtained von Mises stress, von Mises strain, and

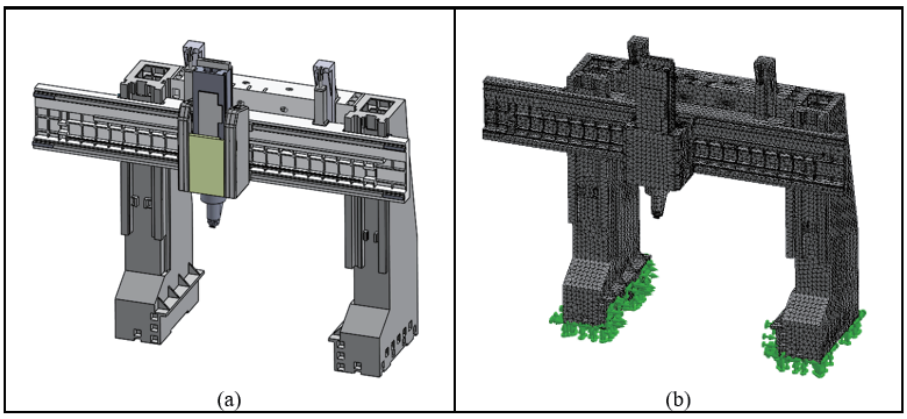

Fig. 3. (Color online) Machine's structure and its meshing results. (a) Structure details. (b) Meshing results.

displacement distributions of the machine structure are shown in Fig. 4. It is found that the maximum von Mises stress and strain are 577.49 kN/m^2 and 3.71 × 10^{-6}, respectively, which are both obtained at the spindle nose [Figs. 4(b) and 4(c)]. The maximum composite displacement is δ_x = 10.36 μm, which is also obtained at the spindle nose [Fig. 4(d)]. The static stiffness of the whole target machine in the X direction can be calculated as K_{sx} = 9.65 kg$_f$/μm, where $K_{sx} = P_x/\delta_x$.

Then, we assume that an external force of P_y = 100 kg$_f$ is applied to the spindle nose in the Y direction. Through calculations via FEM, we obtain the von Mises stress, von Mises strain, and displacement distributions of the target machine, as shown in Fig. 5. The maximum von Mises stress and strain are 713.92 kN/m^2 and 3.85 × 10^{-6}, respectively, which are both obtained at the spindle nose [Figs. 5(b) and 5(c)]. The maximum composite displacement is δ_y = 13.31 μm, which is also obtained at the spindle nose [Fig. 5(d)]. The static stiffness of the whole target machine in the Y direction can be calculated as K_{sy} = 7.51 kg$_f$/μm, where $K_{sy} = P_y/\delta_y$.

Finally, we consider the last circumstance in Case A that the applied force is P_z = 100 kg$_f$. Through FEM calculations, we obtain the von Mises stress, von Mises strain, and displacement distributions of the target machine, as illustrated in Fig. 6. It is observed that the maximum von Mises stress and strain are 323.43 kN/m^2 and 1.76 × 10^{-6}, respectively, which are both obtained at the spindle nose [Figs. 6(b) and 6(c)]. Moreover, it is seen from Fig. 6(d) that the maximum composite displacement of δ_z is 7.51 μm, which is also obtained at the spindle nose [Fig. 6(d)]. The static stiffness of the whole target machine in the Z direction is calculated as K_{sz} = 13.31 kg$_f$/μm, where $K_{sz} = P_z/\delta_z$. Comparing the magnitude of static stiffness for the whole machine

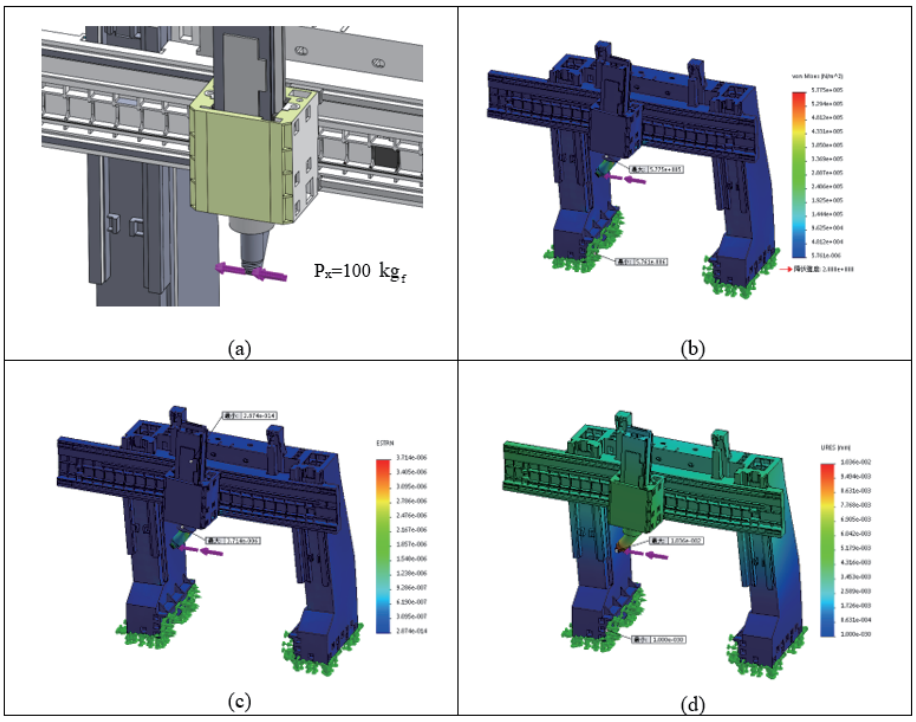

Fig. 4. (Color online) Distributions of stress, strain, and displacement for Case A with P_x = 100 kg$_f$. (a) Applied load. (b) von Mises stress distribution. (c) von Mises strain distribution. (d) Displacement distribution.

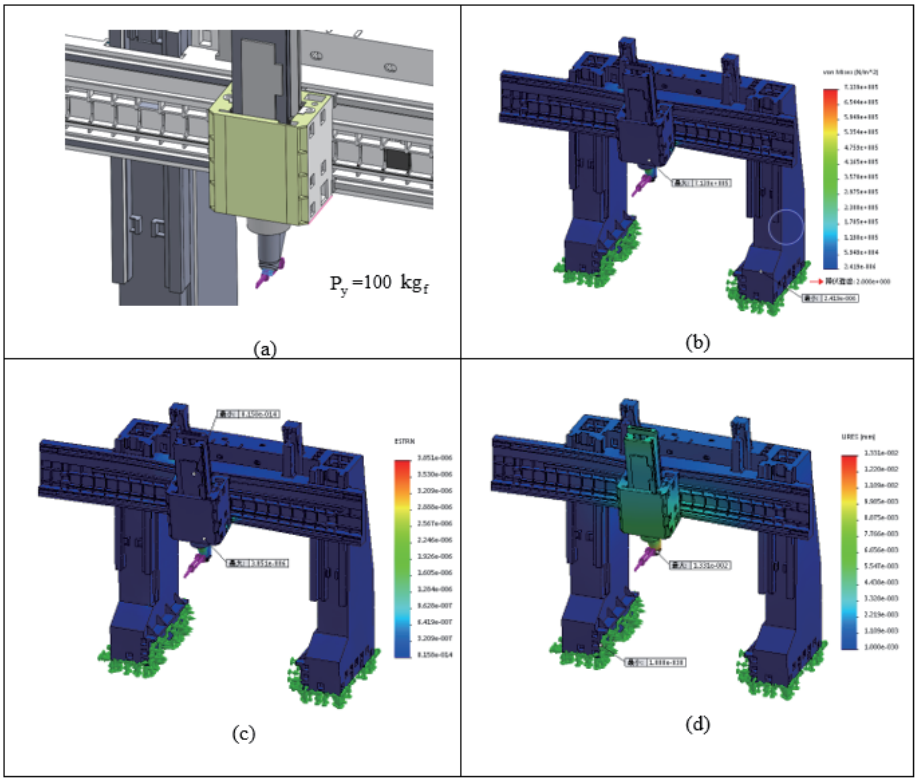

Fig. 5. (Color online) Distributions of stress, strain, and displacement for Case A with P_y = 100 kg_f. (a) Applied lppoad. (b) von Mises stress distribution. (c) von Mises strain distribution. (d) Displacement distribution.

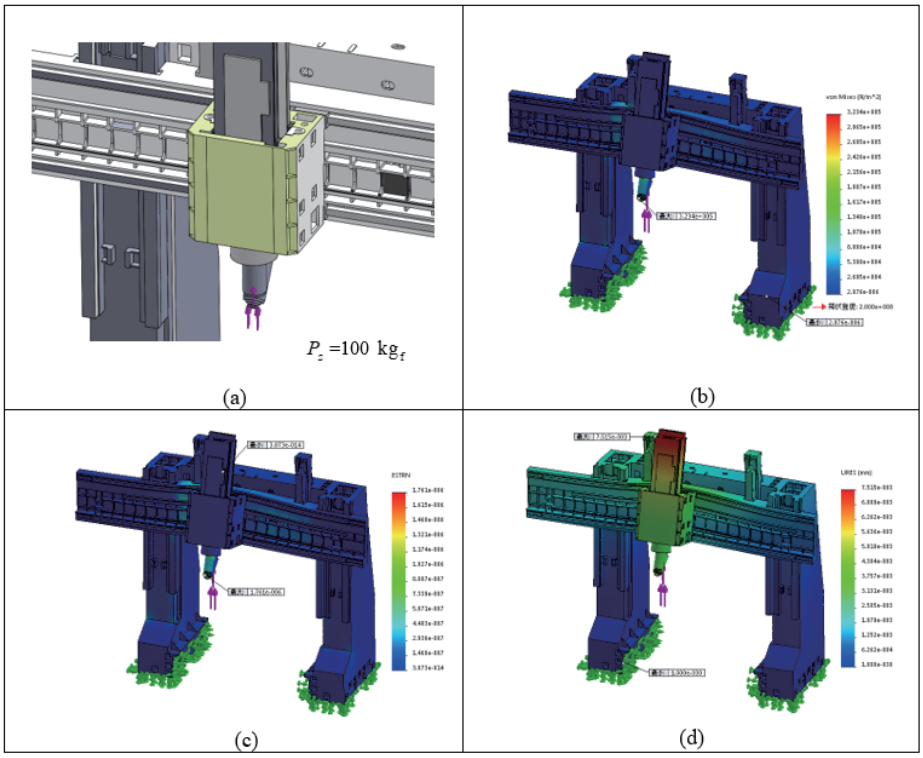

Fig. 6. (Color online) Distributions of stress, strain, and displacement for Case A with P_z = 100 kg_f. (a) Applied load. (b) von Mises stress distribution. (c) von Mises strain distribution. (d) Displacement distribution.

among the above three circumstances in Case A, we obtain the following descending order:

$$K_{sz}\,(13.31) > K_{sx}\,(9.65) > K_{sy}\,(7.51). \tag{11}$$

Since the static stiffness in the *Y* direction (K_{sy} = 7.51 $kg_f/\mu m$) is only about 56% of that in the *Z* direction (K_{sz} = 13.31 $kg_f/\mu m$), it appears that the weakest portion of the whole structure happens in the *Y* direction, and it is suggested that we can improve the structural strength in the *Y* direction by modifying the spindle ram and its back-supporting cross beam.

4.1.2 Mode shape analysis (Case A)

According to Eqs. (3)–(6), we further calculate the natural frequencies of the target MDMC in Case A. To simulate the actual machining conditions, the natural frequencies under investigation are limited below 500 Hz. As such, the FEM-calculated results of 96 natural frequencies are obtained and shown in Table 1. Moreover, to clearly understand the deformation that frequently occurs under resonance conditions, we only demonstrate the first eight modal shapes obtained at frequencies below 80 Hz (corresponding to 4800 rpm), as shown in Fig. 7.

Table 1
Natural frequencies of the whole machine for Case A.

No.	*f* (Hz)	No.	*f* (Hz)	No.	*f* (Hz)	No.	*f* (Hz)
1	21.2	26	191.5	51	294.2	76	414.2
2	21.4	27	199.6	52	298.3	77	417.1
3	32.6	28	200.0	53	302.0	78	420.9
4	45.1	29	212.6	54	304.7	79	423.2
5	48.2	30	217.9	55	314.9	80	431.4
6	53.5	31	222.2	56	324.4	81	432.0
7	62.6	32	223.1	57	327.6	82	434.2
8	75.3	33	226.1	58	333.3	83	441.3
9	82.4	34	234.3	59	339.1	84	444.8
10	85.7	35	242.0	60	345.3	85	450.4
11	102.4	36	247.4	61	349.3	86	453.7
12	104.8	37	249.2	62	349.9	87	460.3
13	111.2	38	251.1	63	361.8	88	466.7
14	115.0	39	258.7	64	367.6	89	475.9
15	119.8	40	264.3	65	374.5	90	480.6
16	131.6	41	266.4	66	375.4	91	483.4
17	139.8	42	269.4	67	381.8	92	485.6
18	141.5	43	271.9	68	389.1	93	486.2
19	151.4	44	274.0	69	392.8	94	492.4
20	162.5	45	277.5	70	397.86	95	496.1
21	166.6	46	278.8	71	398.7	96	499.5
22	168.9	47	280.2	72	399.9		
23	171.6	48	280.9	73	401.9		
24	184.5	49	287.0	74	404.3		
25	190.3	50	289.9	75	410.9		

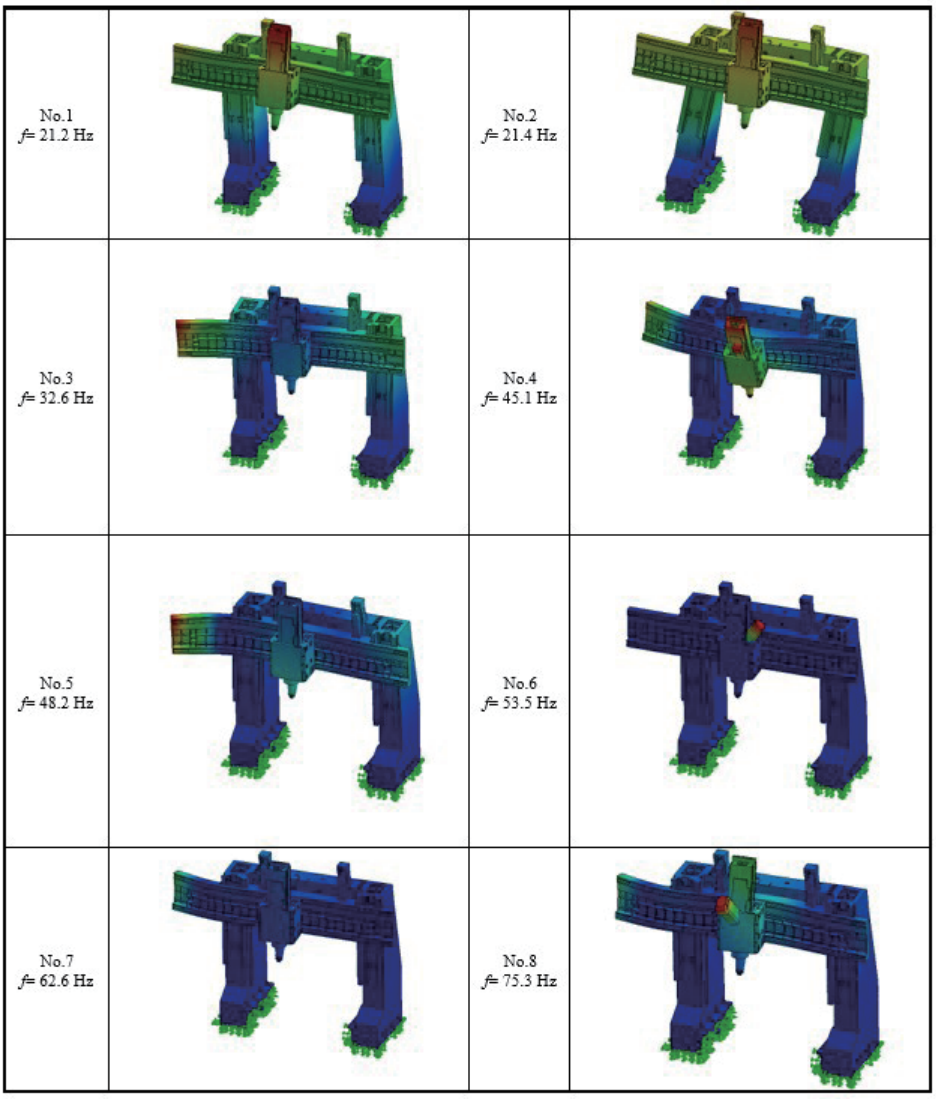

Fig. 7. (Color online) Modal shapes at first eight natural frequencies for Case A.

At the first natural frequency of $f = 21.2$ Hz, the resonance makes the cross beam deform with a forward-and-backward wavy motion. At the second natural frequency of $f = 21.4$ Hz, the resonance makes not only the cross beam deform like in the previous status but also the whole structure vibrates towards the right direction. At the third natural frequency of $f = 32.6$ Hz, the resonance makes the left portion of the cross beam deform forward. At the fourth natural frequency of $f = 45.1$ Hz, the resonance makes the cross beam as well as its attached spindle ram module deform forward and backward. At the fifth natural frequency of $f = 48.2$ Hz, the resonance makes the left portion of the cross beam deform forward. At the sixth natural frequency of $f = 53.5$ Hz, the resonance makes the spindle motor in the ram vibrate toward the right. At the seventh natural frequency of $f = 62.6$ Hz, the resonance makes the left portion of the cross beam deform backward. At the eighth natural frequency of $f = 75.3$ Hz, the resonance makes the left portion of the cross beam deform backward while the spindle motor in the ram vibrates forward.

4.1.3 Dynamic response (Case A)

Since the whole structure is weakest in the *Y* direction (the lowest K_{sy}), we will focus on the dynamic response of the target machine in this direction. We first apply harmonic composite forces to the spindle nose in the *Y* direction with a magnitude of P_y = 100 kg_f and harmonic frequencies in the range of 0–440 Hz. Through FEM calculations based on Eqs. (7)–(10), we obtain the results of local maximum displacements (D_d) and their associated local minimum dynamic stiffness K_d, where $K_d = P_y/D_d$, at different frequencies (f), as listed in Table 2 and drawn in Fig. 8. We found that the global minimum dynamic stiffness, K_d = 0.29 kg_f/μm, is obtained at f = 21.37 Hz. Note that the resonance occurring at this frequency causes a large deformation or serious damage to the whole machine. Moreover, the local dynamic stiffness values obtained at f = 21.24, 297.34, and 312.48 Hz are much smaller than the others (all smaller than 1.0 kg_f/μm). It must be stressed that the machine should not be operated around these specific frequencies to avoid either a large deformation or serious damage during machining.

Second, we apply harmonic composite forces to the spindle nose in the *Y* direction with a magnitude of P_y = 100 kg_f and frequencies in the range of 0–440 Hz. Through FEM calculations based on Eqs. (7)–(10), we obtain the results of local maximum displacements (D_d) and their

Table 2
FEM calculation results of dynamic stiffness in the *X* direction for Case A.

f (Hz)	D_d (μm)	K_d (kg_f/μm)	f (Hz)	D_d (μm)	K_d (kg_f/μm)	f (Hz)	D_d (μm)	K_d (kg_f/μm)
1.59E-06	9.23	10.83	199.92	4.18	23.92	322.12	13.77	7.26
21.24	290.92	0.34	209.67	5.51	18.14	326.85	10.46	9.56
21.37	349.48	0.29	216.69	6.15	16.26	331.98	75.80	1.32
29.98	5.69	17.57	221.18	6.71	14.9	337.71	75.50	1.32
42.17	4.69	21.32	222.86	6.80	14.7	343.8	45.06	2.22
47.44	13.12	7.62	225.40	7.24	13.8	348.32	3.24	30.86
52.23	6.31	15.84	232.35	9.73	10.27	349.73	3.24	30.86
60.48	6.16	16.23	240.17	9.10	10.99	358.98	1.01	99.01
72.35	6.89	14.51	246.12	10.96	9.12	366.23	3.09	32.36
80.71	6.56	15.24	248.76	10.47	9.55	372.86	0.70	142.86
84.90	15.09	6.63	250.62	10.04	9.96	375.17	2.06	48.54
98.48	7.80	12.82	256.93	12.86	7.78	380.25	1.74	57.47
104.25	9.08	11.01	263.00	20.44	4.89	387.39	3.81	26.26
109.71	6.55	15.27	265.91	17.30	5.78	391.93	5.40	18.52
114.12	8.01	12.48	268.69	35.20	2.84	396.67	7.40	13.51
118.71	10.40	9.62	271.29	33.03	3.03	398.51	8.29	12.07
128.86	10.09	9.9	273.52	29.86	3.34	399.64	8.06	12.41
137.88	13.93	7.18	276.69	21.85	4.58	401.41	8.51	11.75
141.06	22.12	4.52	278.47	26.51	3.77	403.69	5.89	16.98
149.07	30.07	3.33	279.83	31.55	3.17	409.33	9.37	10.67
159.92	3.58	27.93	280.71	22.25	4.49	413.4	18.40	5.43
165.46	3.52	28.4	285.53	20.53	4.87	416.39	16.02	6.24
168.28	10.71	9.34	289.19	38.88	2.57	419.97	35.91	2.78
170.94	2.54	39.37	293.18	35.53	2.81	422.63	29.47	3.39
181.48	3.98	25.13	297.34	116.23	0.86	429.46	5.65	17.70
188.91	8.84	11.31	301.10	36.57	2.73	431.86	5.54	18.05
191.21	12.15	8.23	304.09	91.80	1.09	433.65	4.21	23.75
197.72	3.67	27.25	312.48	167.92	0.60	439.65	10.63	9.41

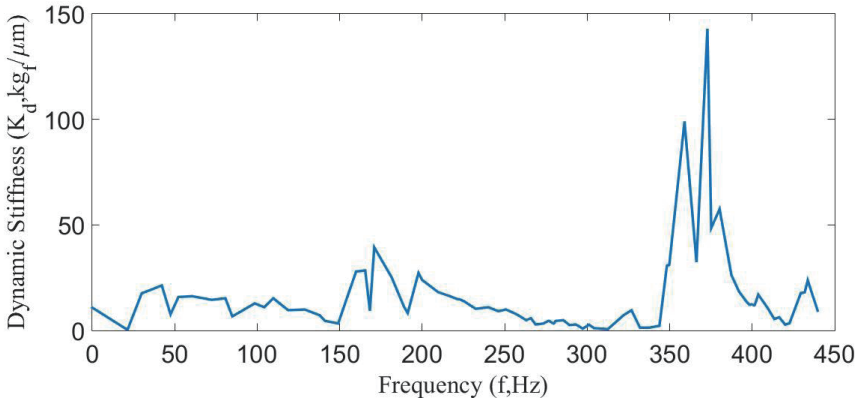

Fig. 8. (Color online) Dynamic stiffness at different external stimulus frequencies (P_x = 100 kg_f).

associated local minimum dynamic stiffness K_d, where $K_d = P_y/D_d$, at different frequencies (f), as listed in Table 3 and drawn in Fig. 9. We found that the global minimum dynamic stiffness K_d = 0.87 kg_f/μm is obtained at f = 21.37 Hz. Note that the resonance occurring at this frequency will cause a large deformation or serious damage to the whole machine structure. Moreover, the local dynamic stiffness values obtained at f = 21.24 and 268.69 Hz are much smaller than the others (all smaller than 1.1 kg_f/μm). It must be stressed that the machine should not be operated around these specific frequencies to avoid either a large deformation or serious damage during machining.

Comparing the global minimum dynamic stiffness Kd values of 0.29 and 0.81 kg_f/μm in the X and Y directions, respectively, we surprisingly found that although the machine has a higher dynamic stiffness in the Y direction than in the X direction, its static stiffness is just the opposite. It must be stressed that, for designing a strong machine, not only a synchronous consideration of the static and dynamic stiffness values is necessary, but also that in different directions is important as well.

4.1.4 Effect of posture on rigidity

4.1.4.1 Case B

Previously, we carried out a detailed investigation on the response of a target machine under static and dynamic stimuli for Case A. Now, we focus on the effect of changing the spindle head position in the ram. When the spindle head locates at the middle position (Case B), we obtain the stress, strain, and displacement distributions by FEM calculations under the same material and boundary conditions as those in Case A. The calculation results are shown in Fig. 10. It is seen that the maximum von Mises stress and strain are 573.07 kN/m^2 and 3.71 × 10^{-6}, respectively, which are both obtained at the spindle nose [Figs. 10(b) and 10(c)]. The obtained maximum composite displacement is 14.13 μm at the spindle nose [Fig. 9(d)]. The static stiffness of the whole target machine in the X direction can be calculated as K_{sx} = 7.08 kg_f/μm on the basis of the applied force and the obtained composite displacement.

Table 3
FEM calculation results of dynamic stiffness in the Y direction for Case A.

f (Hz)	D_d (μm)	K_d (kg_f/μm)	f (Hz)	D_d (μm)	K_d (kg_f/μm)	f (Hz)	D_d (μm)	K_d (kg_f/μm)
1.59E-6	12.60	7.94	199.92	9.33	10.72	322.12	4.16	24.05
21.24	123.57	0.81	209.67	14.66	6.82	326.85	8.59	11.63
21.37	114.64	0.87	216.69	35.74	2.80	331.98	5.07	19.71
29.98	17.93	5.58	221.18	4.56	25.61	337.71	11.38	8.79
42.17	51.76	1.93	222.86	3.15	31.70	343.80	7.19	13.91
47.44	20.01	5.00	225.4	4.55	22.00	348.32	8.62	11.60
52.23	17.43	5.73	232.35	14.56	6.87	349.73	8.63	11.59
60.48	4.63	21.60	240.17	13.36	7.49	358.98	4.23	23.64
72.35	6.47	15.46	246.12	34.58	2.89	366.23	2.36	42.40
80.71	11.86	8.43	248.76	21.96	4.55	372.86	1.09	92.07
84.90	49.87	2.01	250.62	6.43	15.56	375.17	4.40	22.74
98.48	4.42	22.64	256.93	21.70	4.608	380.25	1.56	64.13
104.25	27.64	3.62	263	22.30	4.48	387.39	12.95	7.72
109.71	2.25	44.49	265.91	41.63	2.40	391.93	10.52	9.51
114.12	4.47	22.38	268.69	95.00	1.053	396.67	5.71	17.50
118.71	7.37	13.56	271.29	45.34	2.21	398.51	4.51	22.16
128.86	4.79	20.88	273.52	50.26	1.99	399.64	5.33	18.77
137.88	8.26	12.11	276.69	24.55	4.07	401.41	5.47	18.27
141.06	6.67	14.98	278.47	24.02	4.16	403.69	4.71	21.23
149.07	10.06	9.94	279.83	31.40	3.19	409.33	3.99	25.04
159.92	7.53	13.28	280.71	44.23	2.26	413.4	13.73	7.28
165.46	10.48	9.54	285.53	24.10	4.15	416.39	9.37	10.67
168.28	20.65	4.84	289.19	31.09	3.22	419.97	7.94	12.60
170.94	3.79	26.39	293.18	12.39	8.07	422.63	9.16	10.92
181.48	9.69	10.32	297.34	39.31	2.54	429.46	4.51	22.17
188.91	18.07	5.53	301.1	25.47	3.93	431.86	4.33	23.09
191.21	11.51	8.69	304.09	16.57	6.03	433.65	5.34	18.74
197.72	8.24	12.14	312.48	6.25	15.99	439.65	8.92	11.21

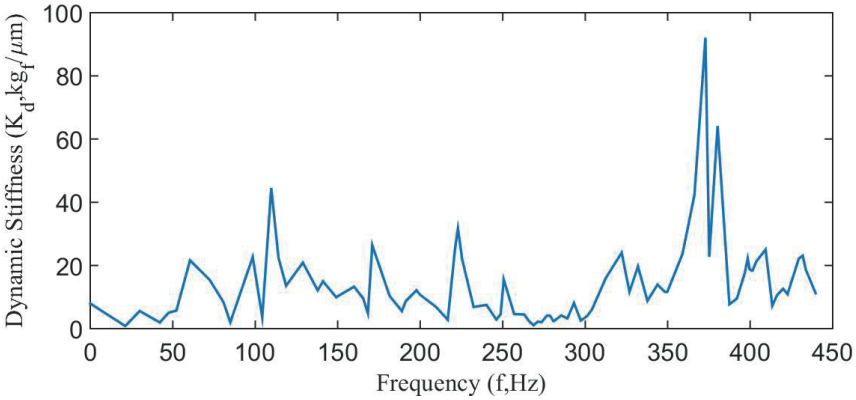

Fig. 9. (Color online) Dynamic stiffness at different external stimulus frequencies (Py = 100 kgf).

Second, we consider an external force of P_y = 100 kg_f applied to the spindle nose in the Y direction. Through FEM calculations, the obtained von Mises stress, von Mises strain, and displacement distributions of the target structure are shown in Fig. 11. The calculated maximum von Mises stress and strain are 705.59 kN/m^2 and 3.82 × 10^{-6}, respectively, which are both

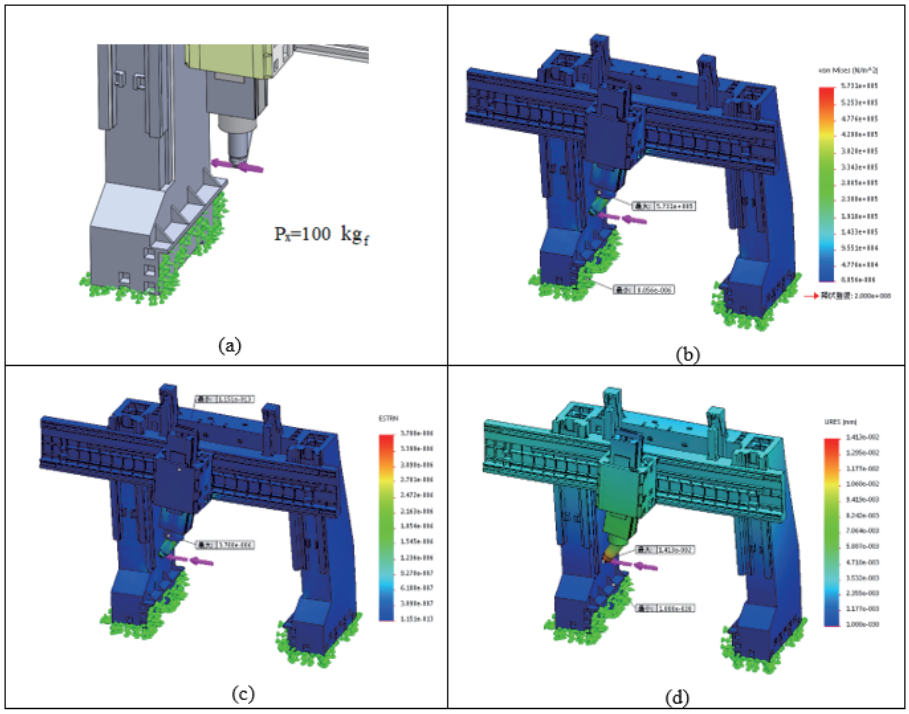

Fig. 10. (Color online) Distributions of stress, strain, and displacement for Case B with P_x = 100 kg_f. (a) Applied load. (b) von Mises stress distribution. (c) von Mises strain distribution. (d) Displacement distribution.

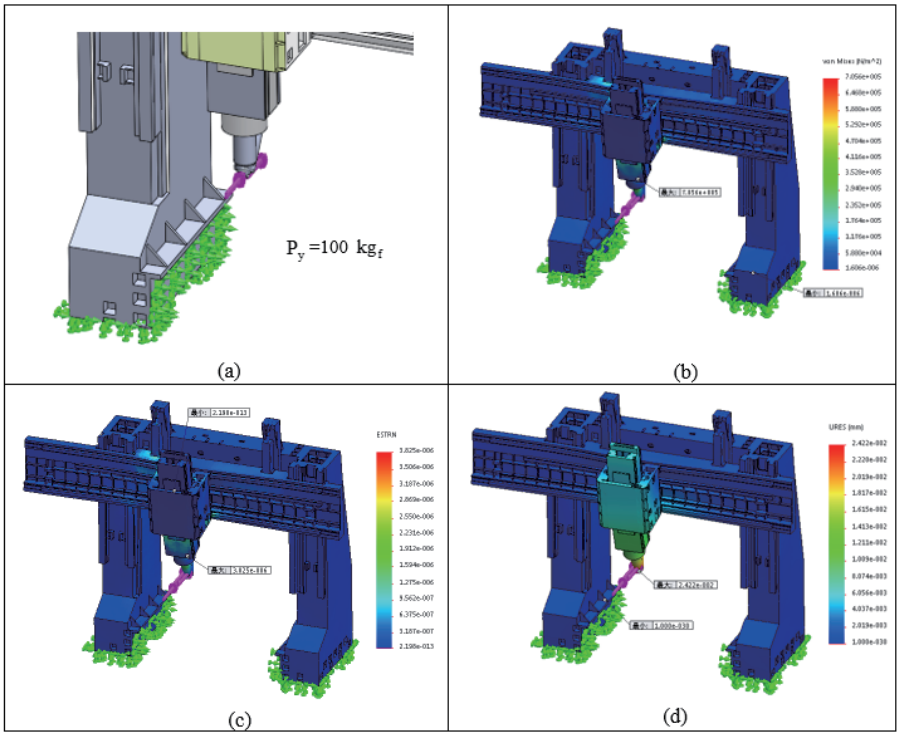

Fig. 11. (Color online) Distributions of stress, strain, and displacement for Case B with P_y = 100 kg_f. (a) Applied load. (b) von Mises stress distribution. (c) von Mises strain distribution. (d) Displacement distribution.

obtained at the spindle nose [Figs. 11(b) and 11(c)]. The obtained maximum composite displacement is 24.22 μm at the spindle nose [Fig. 11(d)]. The static stiffness of the whole target machine in the Y direction can be calculated as K_{sy} = 4.13 $kg_f/\mu m$ on the basis of the applied force and the obtained composite displacement.

Third, we consider an external force of P_z = 100 kg_f applied to the spindle nose in the Z direction. The von Mises stress, von Mises strain, and displacement distributions of the target structure are calculated via FEM and the obtained results are shown in Fig. 12. It appears from Fig. 12 that the maximum von Mises stress and strain are 323.66 kN/m^2 and 1.74 × 10^{-6}, respectively, which are both obtained at the spindle nose [Figs. 12(b) and 12(c)]. The obtained maximum composite displacement is 6.39 μm at the spindle nose [Fig. 12(d)]. The static stiffness of the whole target machine in the Z direction can be calculated as K_{sz} = 15.65 $kg_f/\mu m$ on the basis of the applied force and the obtained composite displacement.

From what we obtained above, we can draw the conclusion that

$$K_{sz}(15.65) > K_{sx}(7.08) > K_{sy}(4.13)\,. \tag{12}$$

Again, the above relation indicates that the static stiffness in the Y direction has the smallest value as in Case A. Therefore, it is suggested that the Y-directional structural strength should be especially increased on the basis of, for example, the geometric shape of the column, the connection way, and the inner rib type, in order to improve the overall structural strength of the whole machine.

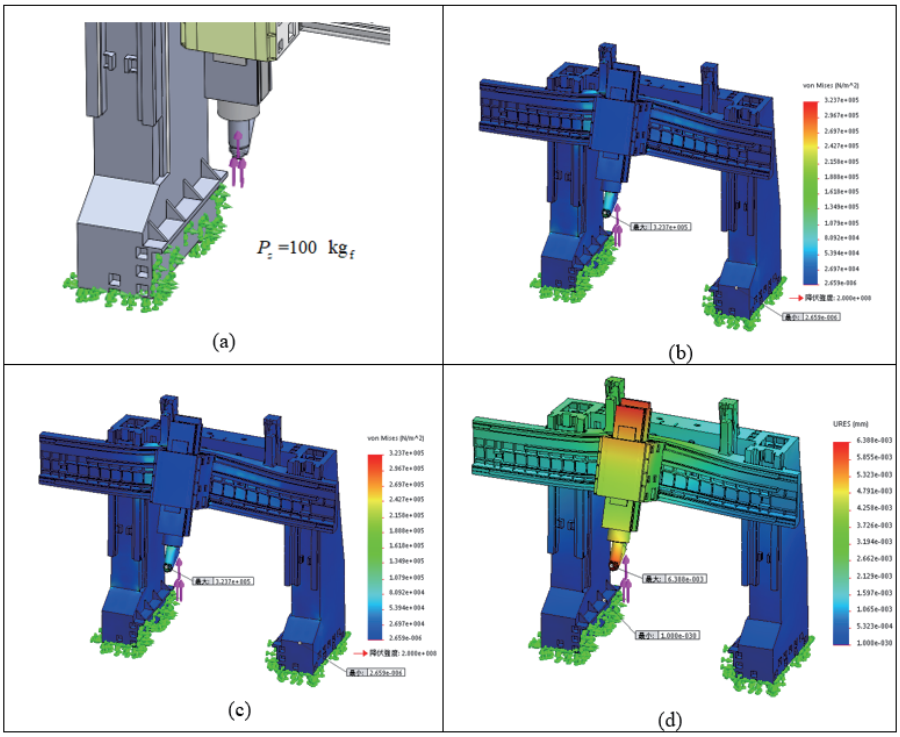

Fig. 12. (Color online) Distributions of stress, strain, and displacement for Case B with P_z = 100 kg_f. (a) Applied load. (b) von Mises stress distribution. (c) von Mises strain distribution. (d) Displacement distribution.

4.1.4.2 Case C

Finally, we consider the posture that the spindle head locates at the bottom position in the ram (Case C). We apply a force of P_x = 100 kg_f to the spindle nose in the X direction [Fig. 13(a)]. The adopted structural material and boundary conditions are the same as in Cases A and B. Through FEM calculations, we obtain the stress, strain, and displacement distributions, as shown in Figs. 13(b)–13(d), respectively. The maximum von Mises stress and strain are 574.89 kN/m^2 and 3.70 × 10^{-6}, respectively, which are both obtained at the spindle nose [Figs. 13(b) and 13(c)]. The obtained maximum composite displacement is 21.9 μm at the spindle nose [Fig. 13(d)]. The static stiffness of the whole target machine in the X direction can be calculated as K_{sx} = 4.57 kg_f/μm on the basis of the applied force and the obtained maximum composite displacement.

Secondly, we consider an external force of P_y = 100 kg_f acting on the spindle nose in the Y direction. Through FEM calculations, the obtained von Mises stress, von Mises strain, and displacement distributions of the target machine are shown in Fig. 14. The calculated results of the maximum von Mises stress and strain are 880.10 kN/m^2 and 4.81 × 10^{-6}, respectively, which are both obtained at the spindle nose [Figs. 14(b) and 14(c)]. The obtained maximum composite displacement is 43.53 μm at the spindle nose [Fig. 14(d)]. The static stiffness of the whole target machine in the Y direction can be calculated as K_{sy} = 2.30 kg_f/μm on the basis of the applied force and the obtained composite displacement.

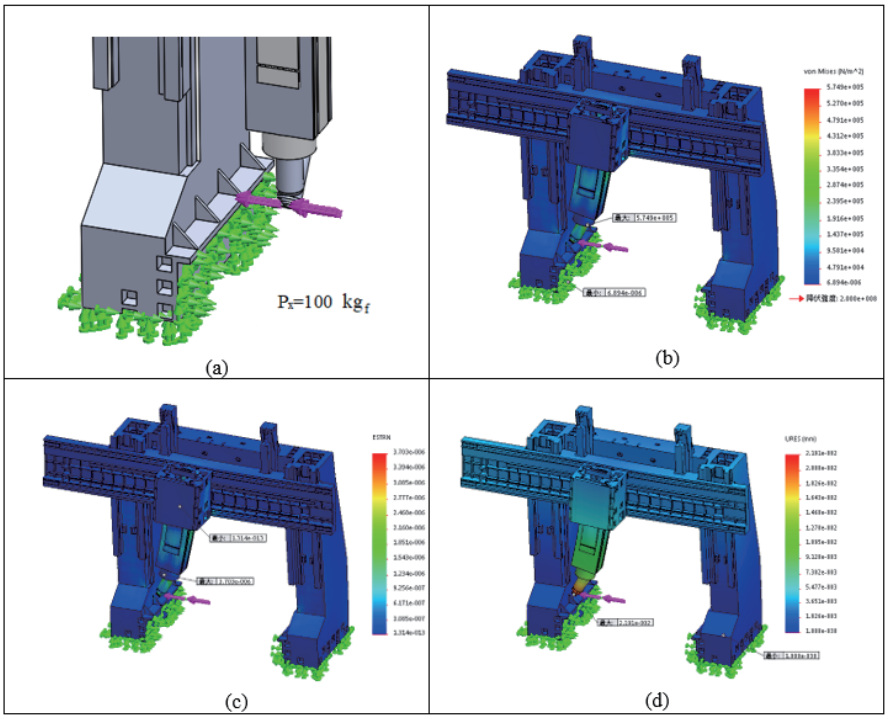

Fig. 13. (Color online) Distributions of stress, strain, and displacement for Case C with P_x = 100 kg_f. (a) Applied load. (b) von Mises stress distribution. (c) von Mises strain distribution. (d) Displacement distribution.

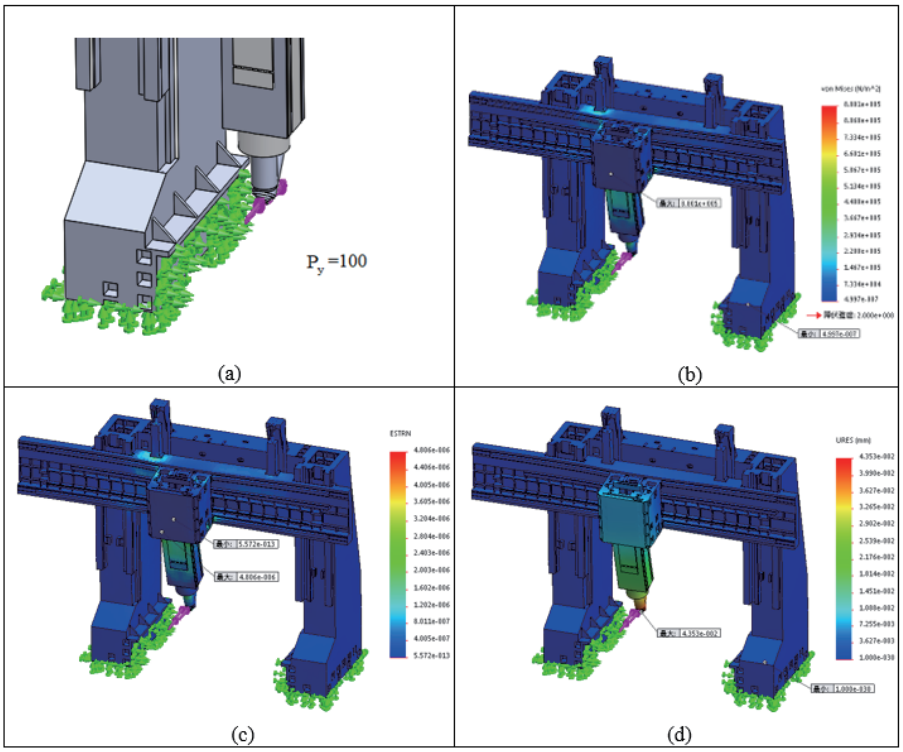

Fig. 14. (Color online) Distributions of stress, strain, and displacement for Case C with P_y = 100 kg_f. (a) Applied load. (b) von Mises stress distribution. (c) von Mises strain distribution. (d) Displacement distribution.

Third, we apply a force of P_z = 100 kg_f to the spindle nose in the Z direction. The von Mises stress, von Mises strain, and displacement distributions of the target machine are obtained via FEM calculations and shown in Fig. 15. The calculated results of the maximum von Mises stress and strain are 327.36 kN/m^2 and 1.79 × 10^{-6}, respectively, which are both obtained at the spindle nose [Figs. 15(b) and 15(c)]. The obtained maximum composite displacement is 8.06 μm at the spindle nose [Fig. 15(d)]. The static stiffness of the whole target machine in the Z direction can be calculated as K_{sz} = 12.41 kg_f/μm on the basis of the applied force and the composite displacement.

From what we obtained above, we can draw the conclusion that

$$K_{sz}(12.41) > K_{sx}(4.57) > K_{sy}(2.30)\,. \tag{13}$$

Again, the above relation indicates that the static stiffness in the Y direction has the smallest value as in Cases A and B. Therefore, it is suggested that the Y-directional structural strength should be especially increased on the basis of, for example, the geometric shape of columns, connection ways, and inner rib types, in order to improve the overall structural strength of the whole machine.

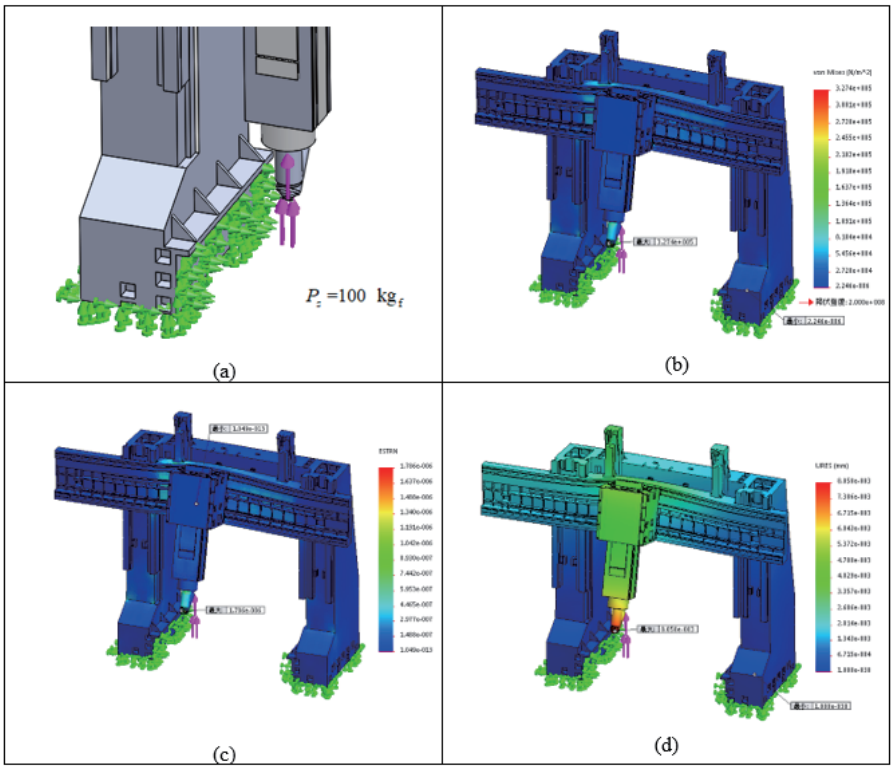

Fig. 15. (Color online) Distributions of stress, strain, and displacement in Case C with P_z = 100 kg_f. (a) Applied load. (b) von Mises stress distribution. (c) von Mises strain distribution. (d) Displacement distribution.

4.2 Experimental Study

4.2.1 Static stiffness measurement

To ascertain that the theoretical results via FEM are convincing, we need to perform an experimental measurement of the related primary parameters. We now build an integrated measurement system to measure the deformation of the target machine under the applied external forces. This measurement system include: (1) a micrometer sensor [Model MAHR 1318 (S/N: 5313180)] with a signal processor [Model AHR Millitron 1202D] with a resolution of 0.01–1 μm; (2) a dynamometer sensor [Model JIHSENSE S-2000 (S/N: 61262)] with a signal processor [Model SGC-2000-500-B-A-P (S/N: 86020067)] with a resolution of 1 kg_f (FEAC Tech); (3) a multichannel dynamic signal analyzer [Model DSPT SigLab 20-42 (S/N: 11234)]; and (4) a module consisting of a force-feeding table, some frames, and a fixed fixture. The built sensor-based deformation measurement system is shown in Fig. 16.

The manipulation procedure of deformation measurement is described as follows. First, we set up related sensors and instruments to construct an integrated measurement system as mentioned earlier. Second, we manually apply forces to the spindle nose via a dynamometer sensor constructed using a force jig mounted on the working table. Third, we detect the displacement of the spindle sleeve via a micrometer sensor.

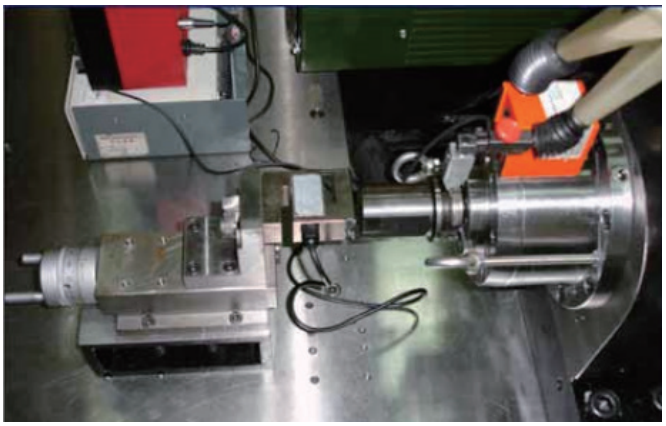

Fig. 16. (Color online) Sensor-based deformation measurement system.

Table 4
Static stiffness data obtained by measurement for Case B.

P_x (kgf)	D_d (μm)	K_{sx} (kgf)	P_y (kgf)	D_d (μm)	K_{sy} (kgf)	P_z (kgf)	D_d (μm)	K_{sz} (kgf)
30	4.27	7.03	30	7.32	4.10	30	1.97	15.24
60	8.68	6.91	60	14.89	4.03	60	3.90	15.38
90	13.39	6.72	90	23.75	3.79	90	5.88	15.30
120	17.54	6.84	120	31.41	3.82	120	7.85	15.28
150	22.03	6.81	150	39.68	3.78	150	10.07	14.89
180	27.27	6.60	180	47.12	3.82	180	12.15	14.82
210	29.70	7.07	210	52.76	3.98	210	14.20	14.79
240	31.58	7.06	240	58.97	4.07	240	16.18	14.83
270	38.96	6.93	270	67.16	4.02	270	17.87	15.11
300	42.37	7.08	300	72.99	4.11	300	19.47	15.41
$\overline{K_{sx}}$ =6.905			$\overline{K_{sy}}$ = 3.952			$\overline{K_{sz}}$ = 15.105		
Simulated static stiffness K_{sx} =7.08			Simulated static stiffness K_{sy} = 4.13			Simulated static stiffness K_{sz} = 15.65		

Regarding the above simulation cases, we typically examine the *X*-, *Y*-, and *Z*-directional static stiffness circumstances in Case B since they are commonly encountered in regular machining. The measured data of applied forces and displacements are shown in Table 4.

4.2.2 Comparison

For Case B, the static stiffness of the target MDMC obtained theoretically in the *X*, *Y*, and *Z* directions has relative errors of 2.53, 4.50, and 3.61%, respectively, with respect to those obtained experimentally. It is worth noting that the machine's static stiffness has a large deviation between the simulated and measured results in the *Y* direction because the column-type structure is inherently weaker in the *Y* direction than in other directions and therefore not easy to accurately predict or measure. The structure of the vertical column tends to deform back and forth when subjected to external applied forces. However, the acceptable measurement results of static stiffness for Case B have shown that our simulation results via FEM are convincing.

Table 5
Comparison of calculated and measured static stiffness values for different types of machine tool.

Machine type	Calculated static stiffness	Measured static stiffness
MDMC (K_{sy}), Case C	4.13 $kg_f/\mu m$	3.952 $kg_f/\mu m$
HMC ($K_{s,whole}$)	3.89 $kg_f/\mu m$	3.60 $kg_f/\mu m$
Relative Error	5.8 %	8.9 %

Table 6
Primary parameters at different spindle head positions (in the *Y* direction).

Spindle head position	σ (kN/m^2)	$\varepsilon \cdot 10^{-6}$	δ (μm)	K_s ($kg_f/\mu m$)	K_d ($kg_f/\mu m$)
Z = 0 mm (Case A)	713.92	3.85	13.31	7.51	0.29
Z = 550 mm (Case B)	705.59	3.82	24.22	4.13	0.23
Z = 1100 mm (Case C)	880.10	4.81	43.53	2.30	0.18

To further verify the correctness of the calculation and measurement results of our target MDMC, we now compare the static stiffness of our target MDMC with that of a large moving-column horizontal machining center machine (HMC),[21] as shown in Table 5. It can be seen that the relative error of the calculated static rigidity between MDMC and HMC is 5.8%, whereas the relative error of the measured static rigidity between them is 8.9%. This comparison result implies that the calculated and measured data of the static rigidity in this study are satisfactory.

4.3 Comparison and optimal structure design

On the basis of the above theoretical results obtained via FEM calculations, we choose the obtained primary parameters in Cases A, B, and C, as listed in Table 6, to investigate the effects of different spindle head positions. The primary parameters in the *Y* direction under consideration include the maximum static von Mises stress, maximum static von Mises strain, maximum static composite displacement, the minimum static stiffness, and the minimum dynamic stiffness. It is seen that changing the extension length of the spindle from Z = 0 to 1100 mm will cause increases of 24.44% in von Mises stress, 24.94% in von Mises strain, and 227.05% in total deformation, and decreases of 69.37% in minimum static stiffness and 37.93% in the minimum dynamic stiffness. The extension length of the spindle head is clearly harmful to the rigidity of the whole machine. To maintain a reliable and highly rigid machining, we should better leverage the function of the moving cross beam (moving upward or downward) instead of extending the spindle head.

5. Conclusion

In this study, we proposed an efficient methodology including CAE and sensor measurement techniques to theoretically and experimentally investigate the structural rigidity of a target MDMC and obtained an optimal design guide of its structure. The effect of the spindle head position on the structural rigidity that significantly affects the static as well as dynamic response

of a column-type machining center was investigated in detail here. Our major findings are summarized as follows.

(1) The structural rigidity of the whole machine markedly decreases with the extension distance of the spindle head (downward direction). A change in the extension length of the spindle head from $Z = 0$ to $Z = 1100$ mm will cause decreases of 69.37% in minimum static stiffness and 37.93% in minimum dynamic stiffness.

(2) The maximum relative error between the experimentally and theoretically obtained results of the machine's static stiffness in the Y direction is 4.5%, which means that the adoption of FEM to analyze the structural rigidity of such a type of machine is satisfactory.

(3) To optimally design a column-type machining center with high static as well as dynamic rigidity, the extension distance of the spindle head in the ram should be as small as possible.

Overall, the novelty of this study is focused on proposing a rapid, economical, and effective methodology to design an optimum column-type machining center. Facing the challenges of ever-increasing functions as well as the complexity of CNC machine tools caused by rapid changes in the market, we should seek more comprehensive methodologies to deal with their structural optimization problems.

Acknowledgments

This work was supported by the Project of the Department of Science and Technology of Fujian Province, China (2021G02013, 2020H0049, 2021H0060), and in part by the Sanming University of Fujian Province, China (19YG05, 19YG04). The authors also acknowledge support from Fujian Provincial University Engineering Research Center for Modern Mechanical Design and Manufacturing Technology, and Fujian Provincial Engineering Research Center for Casting and Forging Parts.

References

1 Q. Ji, C. Li, D. Zhu, Y. Jin, and Y. L. Jixiang: J. Cleaner Prod. **246** (2020) 118976. https://doi.org/10.1016/j.jclepro.2019.118976.C
2 C. Liu, T. Feng, L. Wang, and C. Zhaoyong: J. Mech. Eng. **52** (2016) 161. https://doi.org/10.3901/JME.2016.03.161
3 Z. Ting: Forging Stamping Technol. **35** (2010) 74.
4 Y. Altintas and Y. Cao: CIRP Annals **54** (2005) 379. https://doi.org/10.1016/S0007-8506(07)60127-9
5 J. Heng, G. Yisheng, and Q. Zhicheng: J. Mech. Eng. **47** (2011) 125.
6 T. C. Chen, Y. J. Chen, M. H. Hung, and J. P. Hung: Adv. Mech. Eng. **8** (2016) 1. https://doi.org/10.1177/1687814016656533
7 J. Wang, W. Niu, Y. Ma, L. Xue, and D. Zhang: Int. J. Adv. Manu. Technol. **91** (2021) 545. https://doi.org/10.1007/s00170-016-9721-y
8 Y. Wang, D. Wang, S. Zhang, Z. Tang, L. Wang, and Y. Liu: Chin. J. Aeron. **35** (2021) 485. https://doi.org/10.1016/j.cja.2021.04.001
9 H. Wu, H. Zheng, and X. Li: Int. J. Adv. Manuf. Technol. **109** (2020) 2009. https://doi.org/10.1007/s00170-020-05596-0
10 L. Petrea and G. Stan: IOP Conf. Ser. Mater. Sci. Eng. **1182** (2021) 1. https://doi.org/10.1088/1757-899X/1182/1/012061
11 Z. Lin, W. Tian, D. Zhang, W. Gao, and L. Wang: Int. J. Adv. Manuf. Technol. Sep. 15th (2021). https://doi.org/10.21203/rs.3.rs-893966/v1

12 J. Liu, Y. Cai, H. Zhang, and L. Ding: E3S Web Conf. **252** (2021). https://doi.org/10.1051/e3sconf/202125202036
13 T. N. Ta, Y. L. Hwang, and J. H. Horng: Int. J. Comp. Meth. (2021). https://doi.org/10.1142/S0219876221500286
14 J. J. Wu: Measurement **39** (2006) 740. https://doi.org/10.1016/j.measurement.2006.03.002
15 R. Liusheng, H. Liang, and P. Yongjun: Mach. Des. Res. **26** (2010) 87.
16 M. Guo, X. Jiang, Z. Ding, and Z. Wu: Int. J. Adv. Manuf. Technol. **98** (2020) 2737. https://doi.org/10.1007/s00170-018-2444-5
17 H. Son, H. J. Choi, and H. W. Park: Int. J. Mach. Tools Manuf. **50** (2010) 575, https://doi.org/10.1016/j.ijmachtools.2010.02.006.
18 Y. Shi X. Zhao, H. Zhang, Y. Nie, and D. Zhang: Int. J. Adv. Manuf. Technol. **83** (2016) 1887. https://doi.org/10.1007/s00170-015-7705-y
19 A. Das, S. Shukla, and M. Kumar: Int. J. Adv. Manuf. Technol. **116** (2021) 3489. https://doi.org/10.1007/s00170-021-07533-1
20 K. Jie: J. Human Univ. Arts Sci. **26** (2014) 46.
21 K. C. Wang, C. H. Yang, L. Wu, and H. Gao: Sens. Mater. **32** (2020) 1633. https://doi.org/10.18494/SAM.2020.2681